
# A Multipoint Flux Approximation Method Based Of Harmonic Points (MPFA-H) For The Numerical Simulation Of Coupled Poroelastic Problems

Pedro Victor Paixão Albuquerque[1], Jonathan da Cunha Teixeira[2], Lucíolo Victor Magalhães e Silva[3], Gustavo Lenin Souza Santos Pacheco[4], Fernando Raul Licapa Contreras[5], Paulo Roberto Maciel Lyra[1], Darlan Karlo Elisário de Carvalho[1].

[1]*Departamento de Engenharia Civil - Universidade Federal de Pernambuco*
*Av. Acadêmico Hélio Ramos s/n, CEP: 50670-901, Recife, Pernambuco, Brazil*
*paixao.albuquerque@ufpe.br, darlan.ecarvalho@ufpe.br, paulo.lyra@ufpe.br*
[2]*Centro de Tecnologia (CTEC) - Universidade Federal de Alagoas*
*Av. Lourival Melo Mota s/n, CEP: 57072-900, Maceió , Alagoas*
*jonathan.teixeira@ctec.ufal.br*
[3]*Coordenação de Edificações - Instituto Federal do Sertão de Pernambuco*
*BR-232, Km 508, s/n CEP: 56000-000, Salgueiro, Pernambuco, Brasil*
*luciolo.victor@ifsertao-pe.edu.br*
[4]*Departamento de Engenharia Mecânica - Universidade Federal de Pernambuco*
*Av. Acadêmico Hélio Ramos s/n, CEP: 50670-901, Recife, Pernambuco, Brazil*
*gustavo.lenin@ufpe.br*
[5]*Núcleo de Tecnologia, Centro Acadêmico do Agreste (NT-CAA) - Universidade Federal de Pernambuco*
*Rodovia BR 104 KM 59 s/n, CEP: 55002-970, Caruaru, Pernambuco, Brazil*
*ferlicapac@gmail.com*

**Abstract.** Reservoir simulation is an important tool for the prediction of oil and gas production. However, some physical phenomena were either neglected or oversimplified in the simulations, in order to facilitate the process of developing a simulation tool to analyze the fluid flow within the rock reservoir. One such phenomenon is the mechanical behavior of the reservoir and surrounding rocks, and how it affects rock properties, and consequently, the fluid flow behavior through the porous media, which, in turn, influences its mechanical behavior, since fluid pressure contributes to the rock deformation. These effects are well observed in wellbore stability and reservoir subsidence, as both can severally change the production behavior, if not considered. In this work, Biot's theory of consolidation is used to derive the governing equations of both the process of rock deformation and fluid flow in the porous rock and their coupling. In the petroleum reservoir community, usually, these problems are solved using different numerical methods: The Finite Element Method (FEM) is used for the geomechanics problem while the Finite Volume Method (FVM) is employed for the fluid flow problem. However, in the present paper, we propose a full finite volume formulation for both problems based on the use of the Multi-Point Flux Approximation using Harmonic Points (MPFA-H), which was extended to handle the geomechanical problem. The MPFA-H method is very robust and flexible. Using the same basic strategy for both problems has the advantage of producing a locally conservative formulation, which is important for multiphase flow modeling, and the use of the same data structure which eases the simulation tool development, is expected to increase numerical stability, accuracy, and simulation speed. We use a sequential solution method in which the equations for solid deformation and fluid flow are solved separately and the solutions of each problem exchange information in all time steps, using the fixed-strain split. The solutions obtained with the strategy described are verified using benchmarks found in literature.

**Keywords:** Finite Volume Method, Multipoint flux approximation, Poroelasticity, Reservoir Simulation, Geomechanics.

# 1 Introduction

In the context of Petroleum Reservoir Engineering, phenomena such as borehole collapse and ocean floor subsidence highlighted the necessity to understand how oil production affects the reservoir and surrounding rocks and vice-versa [1]. Those phenomena can impact significantly production behavior which can lead to profit losses and environmental hazards. The presence of a freely moving fluid in a porous rock modifies its mechanical response, which in return, influences the fluid flow inside the pore. This relationship is modelled via the theory of Poroelasticity. In modelling each phenomenon separately, different numerical methods are typically used. For fluid flow inside a porous media, a Finite Volume Method (FVM) is predominately used. On the other hand, in solid deformation problems, a Finite Element Method (FEM) is predominately employed. Using a standard FEM-FVM scheme has several disadvantages due to the different data structures and can even suffer from non-physical oscillations [2] However, in the present work, we propose a unified Finite Volume Framework based on the Multipoint Flux Approximation based on Harmonic Points (MPFA-H)[3, 4], which is very robust and flexible. The MPFA-H is a linear Finite Volume capable of dealing with unstructured polygonal meshes and full diffusion tensors [3, 4]. This unified FVM scheme has several advantages due to the usage of the same data structure and the avoidance of unnecessary interpolations, which is expected to yield faster, more accurate and more stable simulations.

# 2 Mathematical Model

The mathematical model used in the present work is based on Biot's Theory of consolidation, and it's given by the following set of PDE's[5]:

$$\nabla \cdot \underline{\sigma}' - \alpha \nabla p = \overrightarrow{f}. \tag{1}$$

$$S\frac{\partial p}{\partial t} + \nabla \cdot \left( \overrightarrow{v_t} + \alpha \frac{\partial \overrightarrow{u}}{\partial t} \right) = Q_f. \tag{2}$$

where: $\underline{\sigma}'$ is the Effective Cauchy Stress Tensor, $\alpha$ is Biot's coefficient, $p$ is the fluid pressure, $\overrightarrow{f}$ comprises body forces. $S = \phi c_f + (\alpha - \phi)\, c_s$ with $\phi$ is the porosity of the porous media, $c_f$ is the fluid compressibility, $c_s$ is the solid particle compressibility. $\overrightarrow{v_t}$ is the fluid's Darcy Velocity, $\overrightarrow{u}$ is the displacement vector, and $Q_f$ is the source (or sink) term. By assuming linear elasticity and infinitesimal strain, the stress-displacement relationship is given by [6]:

$$\underline{\sigma}' = \underline{\mathbf{C}} : \frac{\nabla \overrightarrow{u} + (\nabla \overrightarrow{u})^{\top}}{2}. \tag{3}$$

where $\underline{\mathbf{C}}$ is the stiffness tensor. Moreover, the relationship between the fluid Darcy Velocity and the Fluid pressure is given by Darcy's Law[7]:

$$\overrightarrow{v_t} = -\frac{1}{\mu}\underline{K}\nabla p. \tag{4}$$

.

A proper set of initial and boundary conditions is given by:

$$\begin{aligned} \overrightarrow{u}(x,t) = \overrightarrow{g}^{u}_{D} \quad in \quad \Gamma^{u}_{D}, \quad \underline{\sigma}' \cdot \overrightarrow{n} = \overrightarrow{g}^{u}_{N} \quad in \quad \Gamma^{u}_{N}, \quad \overrightarrow{u}(x,0) = \overrightarrow{u}_0 \quad in \quad \Omega \\ p(x,t) = g^{p}_{D} \quad in \quad \Gamma^{p}_{D}, \quad \overrightarrow{v_t} \cdot \overrightarrow{n} = g^{p}_{N} \quad in \quad \Gamma^{p}_{N}, \quad p(x,0) = p_0 \quad in \quad \Omega. \end{aligned} \tag{5}$$

where $\overrightarrow{n}$ is the unit outward normal vector to the boundary. The superscript $u$ and $p$ refer, respectively, to the stress equilibrium, eq. (1), and to the storage equation, eq. (2). $\Gamma_D$ denotes the Dirichlet Boundary, with $\overrightarrow{g}_D$ being the prescribed value at the the Dirichlet Boundary. $\Gamma_N$ denotes the Neumann Boundary, with $\overrightarrow{g}_N$being the prescribed value at Neumann Boundary. $\overrightarrow{u}_0$ and $p_0$ are the initial displacement and pressure distributions, respectively.

# 3 Finite Volume Discretezation of Biot Equations

## 3.1 The MPFA method

This work uses a collocated cell-centered finite volume scheme. The first step is to split the computational domain $\Omega$ into $N_{cv}$ computational cells $\hat{L}$. Then, eq. (1) and eq. (2) are integrated in the computational cell.

By integrating the stress divergent, the first term in eq. (1), over the cell $\hat{L}$, and applying the Divergence and Mean Value theorems, we have:

$$\int_{\Omega_{\hat{L}}} \nabla \cdot \underline{\sigma}' \, d\Omega_{\hat{L}} = \int_{\Gamma_{\hat{L}}} \underline{\sigma}' \cdot \overrightarrow{n} \, d\Gamma_{\hat{L}} = \sum_{IJ \in \Gamma_{\hat{L}}} \int_{IJ} \underline{\sigma}' \cdot \overrightarrow{n} \, ds. \tag{6}$$

$$\int_{IJ} \underline{\sigma}' \cdot \overrightarrow{n} \, ds \approx |IJ| \underline{\sigma}' \cdot \overrightarrow{n}_{IJ} = |IJ| \overrightarrow{\mathcal{T}}_{IJ}. \tag{7}$$

where $\Omega_{\hat{L}}$ is the computation cell domain, $\Gamma_{\hat{L}}$ is the computational cell boundary, $IJ$ being the computational cell control surface (edge in 2D), with $|IJ|$ being its size and $\overrightarrow{n}_{IJ}$ being the unit outward normal vector to $IJ$. Furthermore, $\overrightarrow{\mathcal{T}}_{IJ} = \underline{\sigma}' \cdot \overrightarrow{n}_{IJ}$ is known as the traction vector. The traction vector can be written as follows:

$$\overrightarrow{\mathcal{T}}_{IJ} = \left[ \underline{\mathbf{C}} : \frac{\nabla \overrightarrow{u} + \nabla \overrightarrow{u}^{\top}}{2} \right] \cdot \overrightarrow{n}_{IJ} = \begin{bmatrix} \nabla u \cdot \underline{C}^{xx} \overrightarrow{n}_{IJ} + \nabla v \cdot \underline{C}^{xy} \overrightarrow{n}_{IJ} \\ \nabla u \cdot \underline{C}^{yx} \overrightarrow{n}_{IJ} + \nabla v \cdot \underline{C}^{yy} \overrightarrow{n}_{IJ} \end{bmatrix}. \tag{8}$$

where $\underline{C}^{xx}, \underline{C}^{xy}, \underline{C}^{yx}, \underline{C}^{yy}$ are diffusion coefficients constructed from $\underline{\mathbf{C}}$. Therefore, $\underline{C}^{xx} \overrightarrow{n}_{IJ}, \underline{C}^{xy} \overrightarrow{n}_{IJ}, \underline{C}^{yx} \overrightarrow{n}_{IJ}$, $\underline{C}^{yy} \overrightarrow{n}_{IJ}$ are co-normal vectors. Thus, $\nabla u \cdot \underline{C}^{xx} \overrightarrow{n}_{IJ}$, $\nabla v \cdot \underline{C}^{xy} \overrightarrow{n}_{IJ}$, $\nabla u \cdot \underline{C}^{yx} \overrightarrow{n}_{IJ}$ and $\nabla v \cdot \underline{C}^{yy} \overrightarrow{n}_{IJ}$ are diffusion terms that can be approximated via the Multipoint Flux Approximation based on harmonic points (MPFA-H) as it is defined in Contreras et al. [4]. Detailed information on how the harmonic interpolation is defined for the linear elasticity problem can be found in [8]. The second term of eq. (2) is also approximated via the MPFA-H method. Detailed information on how the harmonic interpolation is defined for fluid flow problems can be found in [4].

### 3.2 Time Integration

The numerical integration in the proposed scheme is done via the Implicit Euler Method:

$$\int_{\Omega_{\hat{L}}} S \frac{\partial p}{\partial t} \, d\Omega_{\hat{L}} \approx \frac{V_{\hat{L}} S_{\hat{L}}}{\Delta t} \left( p_{\hat{L}}^{n+1} - p_{\hat{L}}^{n} \right). \tag{9}$$

$$\int_{\Omega_{\hat{L}}} \frac{\alpha}{\partial t} \left( \nabla \cdot \overrightarrow{u} \right) d\Omega_{\hat{L}} \approx \frac{V_{\hat{L}} \alpha_{\hat{L}}}{\Delta t} \left( \nabla \cdot \overrightarrow{u} \Big|_{\hat{L}}^{n+1} - \nabla \cdot \overrightarrow{u} \Big|_{\hat{L}}^{n} \right). \tag{10}$$

where $V_{\hat{L}}$ is the computational cell volume(area in 2D). The superscript $n+1$ and $n$ refer, respectively, to $t_{n+1}$ and $t_n$, with $t_{n+1} = t_n + \Delta t$. All other terms in eq. (1) and eq. (2) are evaluated at $t_{n+1}$.

### 3.3 Pressure-Displacement Coupling

Both the pressure gradient in eq (1) and the displacement divergent in eq (2) are approximated by integrating both terms and then applying the Divergence and Mean Value Theorems:

$$\int_{\Omega_{\hat{L}}} \nabla p \, d\Omega_{\hat{L}} \approx \sum_{IJ \in \Gamma_{\hat{L}}} |IJ| p_{IJ} \overrightarrow{n}_{IJ}, \quad \int_{\Omega_{\hat{L}}} \nabla \cdot \overrightarrow{u} \, d\Omega_{\hat{L}} \approx \sum_{IJ \in \Gamma_{\hat{L}}} |IJ| \overrightarrow{u}_{IJ} \cdot \overrightarrow{n}_{IJ}. \tag{11}$$

where $p_{IJ}$ and $\overrightarrow{u}_{IJ}$ are computed in their respective harmonic points.

The coupling between pressure and displacement is done via the Fixed-Strain Operator Split [9]. At each time step, the solution is obtained by first solving the fluid-flow problem with constant volumetric deformation rate, eq. (10), then the solid mechanics problem is solved with a frozen pressure field. This cycle repeats until convergence is achieved. This choice of the operator split was based on the ease of implementation and natural migration towards a better operator split, the Fixed-Stress Split. The Fixed-Strain split is conditionally stable [9].

## 4 Numerical Results

### 4.1 Terzaghi's Problem

Terzaghi's Problems consists of a homogeneous poroelastic column with height $H$ and length $L$, where, at its top, a load $\sigma_0$ is applied and drainage occurs [10]. Its sides are impermeable and are prevented from lateral movement. Its bottom portion is fixed and also impermeable. Thus, the column has a displacement only in the vertical direction. The analytical solution for this problem can be found in Wang [10]. The meshes used

to solve this problem are shown in Figure 1. Material properties can be found in Table 1. The load applied is $\sigma_0 = -1 \times 10^6\ Pa$.

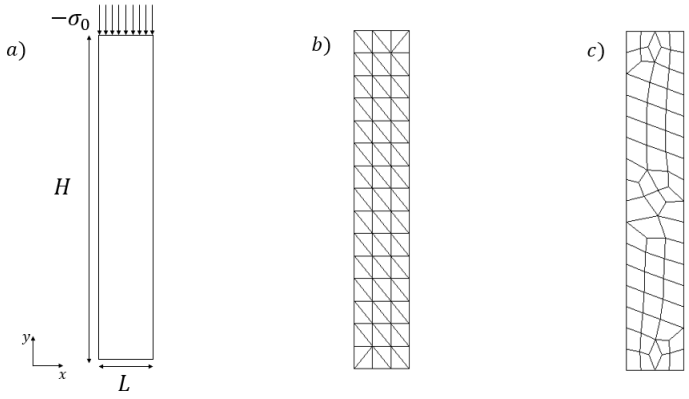


Figure 1. Terzaghi's Problem - $a$) Problem schematic $b$) Mesh 1 - unstructured with triangular elements; $c$) Mesh 2 - unstructured with quadrilateral elements.

Table 1. Terzaghi's Problem - Solid and fluid properties.

| Property | Value |
|---|---|
| Solid Compressibility ($c_s$) | $2.777778 \times 10^{-11}\ Pa^{-1}$ |
| Young's Modulus ($E$) | $14.4 \times 10^9\ Pa$ |
| Poisson's Coefficient ($\nu$) | $0.2$ |
| Porosity ($\phi$) | $0.19$ |
| Permeability ($k$) | $1.9 \times 10^{-15}\ m^2$ |
| Biot's Coefficient ($\alpha$) | $0.777778$ |
| Fluid Compressibility ($c_f$) | $3.030303 \times 10^{-10}\ Pa^{-1}$ |
| Viscosity ($\mu$) | $1 \times 10^{-3}\ Pa.s$ |

Figure 2 and Figure 3 shows a comparison between the numerical and analytical solutions with a $\Delta t = 1\ s$. From their analysis, one can conclude that the numerical formulation presented in this work is capable of accurately match the problem's analytical solution, with both unstructured triangular and quadrilateral meshes. Figure 4 shows the displacement field expected behavior. The displacement is only vertical and it is bigger closer to the top, where the load is applied.

Figure 2. Terzaghi's Problem - Comparison between analytical and numerical solutions for Mesh 1.

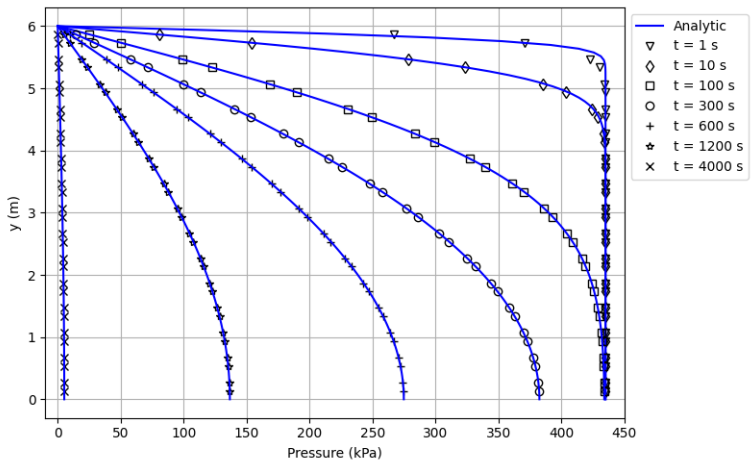

Figure 3. Terzaghi's Problem - Comparison between analytical and numerical solutions for Mesh 2 .

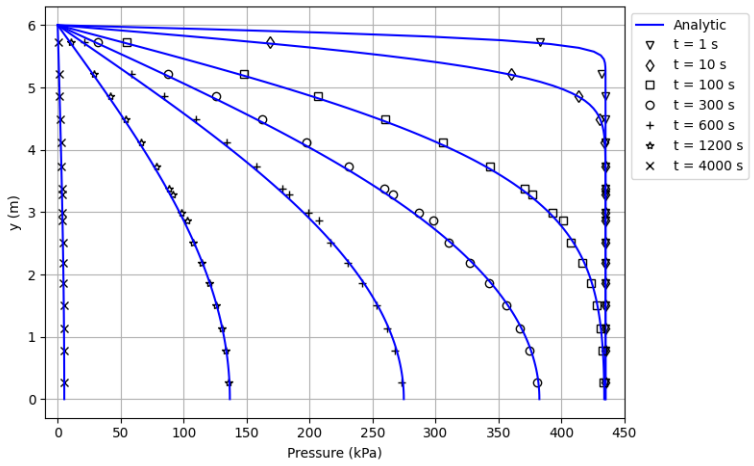


Figure 4. Terzaghi's Problem - Displacement profiles at different times.

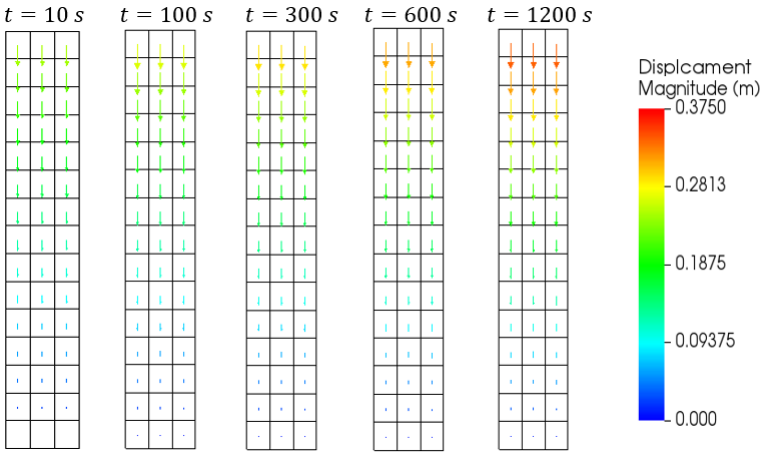


## 4.2 Mandel's Problem

Mandel's Problem consists of a porous media, with height $2H$ and length $2L$, sandwiched between two frictionless, impermeable plates [11]. A vertical force $2F$ is applied at the plates and the sample is drained from the sides, where it is free to deform. Due to the symmetry of the problem, the computational domain can be reduced as shown in Figure 5. The analytical solution can be found in Abousleiman et al. [11]. A structured quadrilateral mesh with a resolution of 30x6 was used in the simulation. The force applied is $F = -1 \times 10^6 N$. Material properties can be found in Table 2.

Figure 5. Mandel's Problem - Domain Reduction.

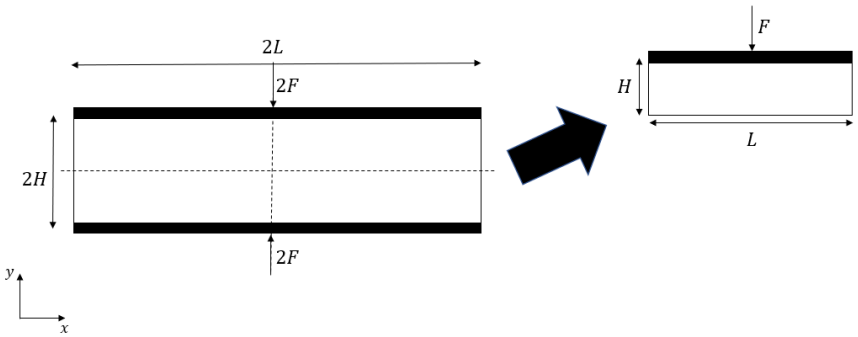

Table 2. Mandel's Problem - Solid and fluid properties.

| Property | Value |
|---|---|
| Solid Compressibility ($c_s$) | $0\ Pa^{-1}$ |
| Young's Modulus ($E$) | $5 \times 10^9\ Pa$ |
| Poisson's Coefficient ($\nu$) | 0.3 |
| Porosity ($\phi$) | 0.3 |
| Permeability ($k$) | $1 \times 10^{-13}\ m^2$ |
| Biot's Coefficient ($\alpha$) | 1 |
| Fluid Compressibility ($c_f$) | $4.5 \times 10^{-9}\ Pa^{-1}$ |
| Viscosity ($\mu$) | $1 \times 10^{-3}\ Pa.s$ |

Figure 6 shows a comparison between the numerical and analytical solutions for Mandel's Problem. Figure 7 shows the pressure profiles at times $t = 10$, $t = 75$, $t = 200$, $t = 500$. Figure 8 shows the displacement distributions at time $t = 500\ s$. From Figure 6, one can conclude that the numerical method is capable of producing accurate solutions for the problem simulated.

Figure 6. Mandel's Problem - Comparison between analytical and numerical solutions with $\Delta t = 1\ s$.

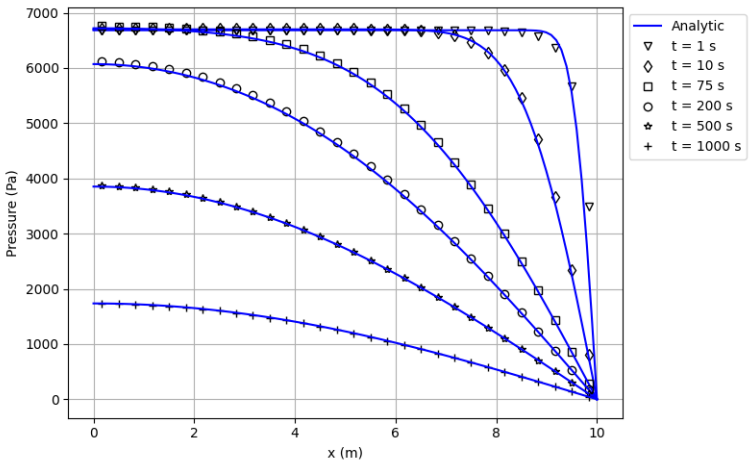


Figure 7. Mandel's Problem - Pore pressure distribution at different times with $\Delta t = 1\ s$.

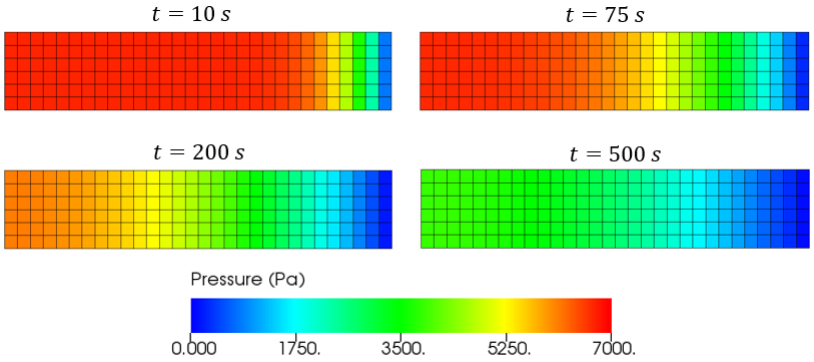

Figure 8. Mandel's Problem - Displacement field at $t = 500$ with $\Delta t = 1\ s$.

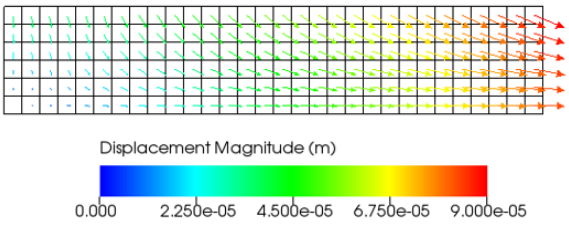


## 5 Conclusions

In the present paper, we present a unified Finite Volume Framework for solving poroelasticity problems based on the Multipoint Flux Approximation method based on harmonic points (MPFA-H) and the Fixed-Strain operator split. The proposed numerical scheme is capable of producing accurate results for the benchmark problems tested, with structured and unstructured meshes. In the near future, we intend to extend the formulation presented to 3D, and include more complex physical phenomena, such as elastoplastic deformation, and numerical improvements, such as changing the pressure-displacement coupling methodology and introducing a non-linear finite volume formulation to avoid violations of the Discrete Maximum Principle.

**Acknowledgements.** The authors would like to thank the Conselho Nacional de Desenvolvimento Cientıfico e Tecnológico – CNPq, Coordenação de Aperfeiçoamento de Pessoal de Nıvel Superior - CAPES and Energi/Simulation.

**Authorship statement.** The authors hereby confirm that they are the sole liable persons responsible for the authorship of this work, and that all material that has been herein included as part of the present paper is either the property (and authorship) of the authors, or has the permission of the owners to be included here.

## References

[1] M. D. Zoback. *Reservoir geomechanics*. Cambridge university press, 2010.
[2] R. Asadi and B. Ataie-Ashtiani. Numerical modeling of subsidence in saturated porous media: A mass conservative method. *Journal of hydrology*, vol. 542, pp. 423–436, 2016.
[3] Z.-M. Gao and J.-M. Wu. A linearity-preserving cell-centered scheme for the anisotropic diffusion equations. In *Finite Volumes for Complex Applications VII-Methods and Theoretical Aspects*, pp. 293–301. Springer, Switzerland, 2014.
[4] F. R. L. Contreras, M. R. A. Souza, P. R. M. Lyra, and D. K. E. Carvalho. A mpfa method using harmonic points coupled to a multidimensional optimal order detection method (mood) for the simulation of oil-water displacements in petroleum reservoirs. *Revista Interdisciplinar de Pesquisa em Engenharia*, vol. 2, n. 21, pp. 76–95, 2017.
[5] M. A. Biot. General theory of three-dimensional consolidation. *Journal of applied physics*, vol. 12, n. 2, pp. 155–164, 1941.
[6] W. S. Slaughter. *The linearized theory of elasticity*. Springer Science & Business Media, 2012.
[7] R. E. Ewing. *The mathematics of reservoir simulation*. SIAM, 1983.
[8] K. M. Terekhov and H. A. Tchelepi. Cell-centered finite-volume method for elastic deformation of heterogeneous media with full-tensor properties. *Journal of Computational and Applied Mathematics*, vol. 364, pp. 112331, 2020a.
[9] J. Kim, H. A. Tchelepi, and R. Juanes. Stability and convergence of sequential methods for coupled flow and geomechanics: Fixed-stress and fixed-strain splits. *Computer Methods in Applied Mechanics and Engineering*, vol. 200, n. 13-16, pp. 1591–1606, 2011.
[10] H. Wang. *Theory of linear poroelasticity with applications to geomechanics and hydrogeology*, volume 2. Princeton university press, 2000.
[11] Y. Abousleiman, A. H. D. Cheng, L. Cui, E. Detournay, and J. C. Roegiers. Mandel's problem revisited. *Geotechnique*, vol. 46, n. 2, pp. 187–195, 1996.